European Geothermal Congress 2013
Pisa, Italy, 3-7 June 2013

Evidence of fractures on seismic data for geothermal exploration

Aleardi Mattia[1], Tognarelli Andrea[1], Mazzotti Alfredo[1] , Ciuffi Simonetta[2], Casini Michele[2]

[1] University of Pisa, Earth Sciences Department, Via S. Maria 53, 56126 Pisa (Italy)

[2] Enel Green Power, Via Andrea Pisano 120, 56122 Pisa (Italy)

mattia.aleardi@for.unipi.it

Keywords: fractures, seismic, exploration, attributes, geothermal.

ABSTRACT

The deep geothermal reservoirs in the Larderello-Travale field (southern Tuscany) are found in intensively fractured portions of intrusive/metamorphic rocks. Therefore, the geothermal exploration carried out by Enel Green Power has been in search of possible fracture signatures that could be retrieved from the analysis of geophysical data. In the present work, thanks to the availability of borehole logs and 3D seismic data, we assess the feasibility of finding seismic markers which may pinpoint fractured levels. These seismic markers include either pre-stack and post-stack reflection attributes and they all require tailored seismic processing sequences to correct for amplitude and phase distortions, noise contamination and to preserve azimuthal and offset variations.

1. INTRODUCTION

Continental extensional tectonic environments with high heat flow are often affected by geothermal systems, independently from the geodynamic context in which they are located (Barbier, 2002; Batini et al. 2003). Extension also characterizes southern Tuscany (inner Northern Apennines), where the most important geothermal fields of Italy are located. Larderello-Travale is one of these and its structural setting is a consequence of two contrasting processes: the first one is connected to the convergence and subsequent collision between the European and African margin (Late Cretaceous - Early Miocene) (Boccaletti and Guazzone, 1972; Boccaletti et al., 1981); the second process is instead connected to the extensional tectonics which affected the inner part of the Northern Apennines since Miocene (Carmignani and Klingfield, 1990; Jolivet et al., 1990; Bertini et al., 1991; Baldi et al., 1994b; Carmignani et al., 1994, 1995; Jolivet et al., 1998). Extensional tectonics is joined with the emplacement of igneous rocks deriving by the mixing of crustal and mantle magmas. Southern Tuscany is presently characterized by high heat flow: 120 mW/m² on average, with local peaks up to 1000 mW/m² (Batini et al. 2003, Bertini et al. 2006).

In this study we verify if a complex system of interconnected fractures hosting a geothermal reservoir gives rise to a distinct and discernible seismic signature.

We focus our attention on complex seismic attributes, AVA (Amplitude Versus Angle) and AVAZ (Amplitude Versus Azimuth) analysis, which have become important tools for hydrocarbon prospecting and they are also used in geothermal exploration (Mazzotti et al., 2002; Casini et al., 2009; Casini et al., 2010).

Since their introduction in the early 1970's, Complex Seismic Trace Attributes have gained considerable popularity, first as a convenient display form, and later, as they were incorporated with other seismically-derived measurements, they became a valid analytical tool for lithology prediction and reservoir characterization (Taner et al., 1979; Mazzotti, 1991).

For what concerns the various AVA techniques, they have been mainly applied in clastic lithologies for hydrocarbon exploration (Ostrander, 1984; Rutherford and Williams, 1989; Mazzotti, 1990; Mazzotti, 1991; Fatti et al., 1994; Aki and Richard, 1980, among others) and few examples refer to carbonate reservoirs (Adriansyah and McMechan., 2001; Shen et al., 2002). Therefore the AVA response of a massive intrusive rock, locally characterized by interconnected fractures, as it is the case of the deep basement rocks of the geothermal field in the Larderello-Travale area, is largely unknown.

AVAZ is a relatively new seismic method that is gaining popularity amongst those investigating fractured reservoirs. Vertically aligned fractures (HTI media) can influence the propagation velocity of seismic waves in the earth. As a consequence, the strength of the seismic response varies not only with

incident angle (as shown in the conventional AVA method), but also with azimuth. AVAZ is based on the study of wave propagation which models amplitudes in terms of azimuth, incident angle and three additional anisotropic parameters which characterize the fracture intensity and orientation (Thomsen, 1986). In the mid 1990's, it began to be shown that there are measurable differences in the seismic AVA responses parallel and perpendicular to fractures, (e.g. Lynn et al. 1996, Mallick et al., 1998), suggesting that AVAZ would be a viable technology. In the late 1990's, AVAZ began to be used on 3D datasets and quickly provided evidence of its importance (e.g. Gray et al., 1999).

To demonstrate the potentials and the limits of these methods, we make use of well-logs (density, *Vp, Vs*) from three wells in the Larderello-Travale area, of synthetic seismograms computed on log-derived models and of real 3D seismic pre-stack and stack data. In the following sections, besides brief recalls of complex attribute, of the linear AVA method and of the AVAZ methodology, we first illustrate the available well logs, and the changes in density and seismic velocities due to the fractured intervals. Then we consider velocity and density logs of wells that drilled different fractured zones to derive depth models on which to compute synthetic seismic data by means of simple convolutional theory (for post-stack attributes) and of the reflectivity method (for pre-stack attributes). Calibration with the check shots and proper downscaling from log to seismic scale were first carried out making use of the Backus averaging method (Backus, 1962).

2. AVAILABLE LOG AND SEISMIC DATA

Figures 1, 2 and 3 show the density, *Vp*, and *Vs* logs pertaining to the three wells used in this work. Each fracture is highlighted by a dotted red line and it is indicated with a number from 1 to 5. Observing these figures we can appreciate that the fractured zones produce a strong decrease of density, and also a decrease of *Vp* and *Vs*. In particular, the density shows a sharp decrease that in the log appears as a spike at the fracture location, indicating the very small width of the fractured zone.

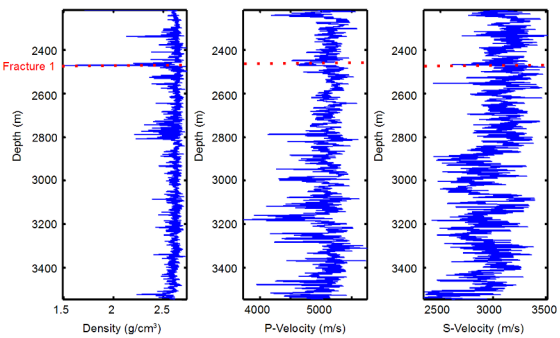

Figure 1: Density, P-wave velocity and S-wave velocity logs pertaining to Well 1. The dotted red line indicates the fracture position.

This observation, combined with the information from the drilling log, that indicates a sudden drop of the drill string in correspondence of the fractured zones, allow us to infer that the fractures appear as "*gaps*" of very limited thickness inside the igneous rock.

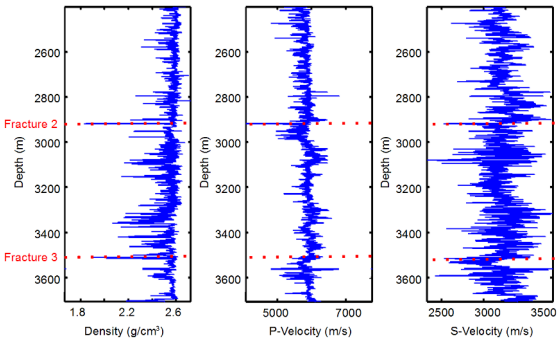

Figure 2: Density, P-wave velocity and S-wave velocity logs pertaining to Well 2. The dotted red lines indicate the fracture positions.

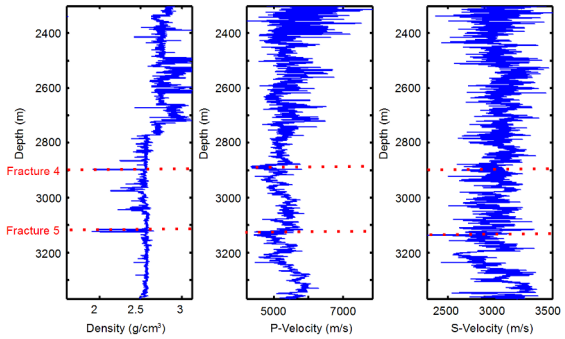

Figure 3: Density, P-wave velocity and S-wave velocity logs pertaining to Well 3. The dotted red lines indicate the fracture positions.

A total of 60 km^2 of 3D seismic data were acquired in the Larderello-Travale area. The orthogonal geometry acquisition is based on 6-receiver lines with an othogonal source line of six shot points. The receiver lines, each formed by 120 channels spaced 50 m, are separated by 480 m. While the source lines are spaced 500 m with a source interval of 80 m. The resulting 25X40 m common midpoint bins yield a 1800% nominal fold covering offsets that range between 47 m and 3500 m. A total length of 8 s was recorded using a 2 ms sample rate. For the purpose of this project, only the shallowest part (i.e. down to 4 s) is considered in this work.

The acquired seismic data is processed paying particular attention in preserving the true amplitudes of the signal. To this end, the processing sequence applied includes amplitude corrections and surface consistent operators and no gain functions or algorithms that potentially could alter the true amplitude response of the signal.

Even though the processing sequence is aimed at recovering the true amplitude of the signal and at enhancing the S/N ratio, the problematic static corrections related to the very rough topography (that ranges from 300 up to 1000 m), in addition to the residual ground-roll contaminating the band of

interest, and the extremely complex geology of the investigated area, allow us to be more confident on post-stack attributes than on pre-stack attributes. In fact the summation among traces that takes place passing from pre-stack to stack domain, considerably increase the quality of the seismic data. Accordingly, the information extracted from the stacked traces are usually more effective and robust than those extracted from the pre-stack domain, which is more sensitive to residual noise contamination. Therefore, in the following sessions we first derive and compare the synthetic and the real seismic post-stack responses of the fractured levels. But, for what concerns the pre-stack domain, we perform only a feasibility study, trying to evaluate the expected AVA and AVAZ signatures of the fractured intervals. In this case we make use of the acquired density and velocity logs, of theoretical formulas and of synthetic seismic data.

3. A BRIEF REVIEW OF COMPLEX SEISMIC ATTRIBUTES

Complex trace analysis treats a seismic trace *f(t)* as the real part of an analytical signal:

$$F(t)=f(t)+jf'(t) \qquad [1]$$

The analytical trace *F(t)* is uniquely determinable from *f(t),* being *jf'(t)* the Hilbert transform of *f(t)*. The most used attributes are reflection strength *A(t)*, instantaneous frequency *w(t)*, and instantaneous phase *θ(t)*:

$$A(t)=\sqrt{(f^2(t)+f'^2(t))} \qquad [2]$$

$$\theta(t)=\tan^{-1}(f'(t)/f(t)) \qquad [3]$$

$$w(t)=\frac{d\theta(t)}{dt} \qquad [4]$$

High-reflection strength is often associated with major lithologic changes between adjacent rock layers, such as across unconformities and boundaries. High-reflection strength also is often associated with gas accumulations. The instantaneous phase, defined by equation (3), emphasizes the continuity of events while the instantaneous frequency may pinpoint subtle low frequency shift of the seismic signal often due to absorption effects, while high frequency shift may be associated with interference phenomena due to thin layer.

4. COMPLEX SEISMIC ATTRIBUTES ON SYNTHETIC AND REAL STACK TRACES

After converting log data from depth to time using check-shot data and after downscaling the recorded logs to the seismic sample interval (2 ms), we use the *Vp* and density logs to compute the zero offset reflectivity trace pertaining to each well. The normal incidence synthetic seismic traces are computed convolving the reflectivity series with a 20 Hz Ricker wavelet. The following step is to extract the real seismic traces corresponding to each well. Due to the deviation of the well tracks, we have considered a small 3D volume around each well, from which we have extracted the real seismic traces with the best correlation with the synthetic ones. The match between the synthetic and the real traces is fairly good, especially near the fractured intervals, as shown in Figure 4. From these traces is clearly evident that the fractured intervals produce a strong negative seismic amplitude at normal incidence, due to the strong decrease in density and P-wave velocity, which occurs passing from the tight rock to the fractured level.

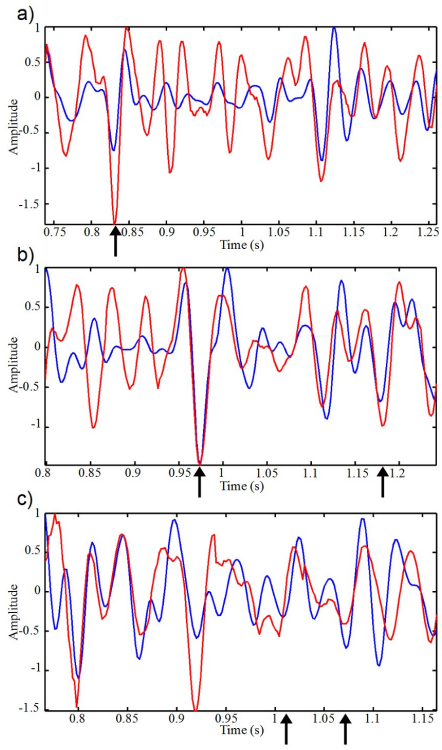

Figure 4: Comparison between the synthetic (in blue) and the extracted (in red) seismic traces (after amplitude normalization) pertaining to Well 1, 2 and 3 (part a, b and c, respectively). The black arrows indicate the time position of each fracture. Note the fairly good match between the synthetic and the real stack traces.

The complex seismic attributes reflection strength and instantaneous frequency are computed both on the synthetic and on the extracted real traces. These attributes show (Figures 5, 6 and 7) that the fractured intervals are often associated with high values of the reflection strength attribute (observable either on synthetic and real traces), which are produced by the abrupt change in physical properties at the interface separating the intrusive rock and the fractured zone. Conversely, instantaneous frequency does not show any anomalous behaviour probably due to the limited thickness and extension of the fractured interval. Similar results are obtained from the computation of the complex attributes on the seismic volume. Reflection strength allows to identify the main petrophysical contrasts, while the instantaneous frequency does not point out any correlation with the fractured levels (Figure 8).

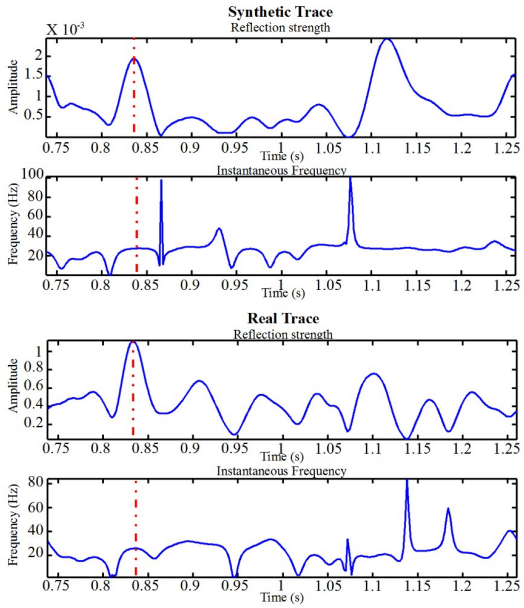

Figure 5: Comparison between complex attribute reflection strength and instantaneous frequency computed on synthetic and real seismic trace for Well 1. The dotted red lines indicate the temporal position of the fractured interval. Note the anomalous high amplitude of the reflection strength produced by the fractured zone.

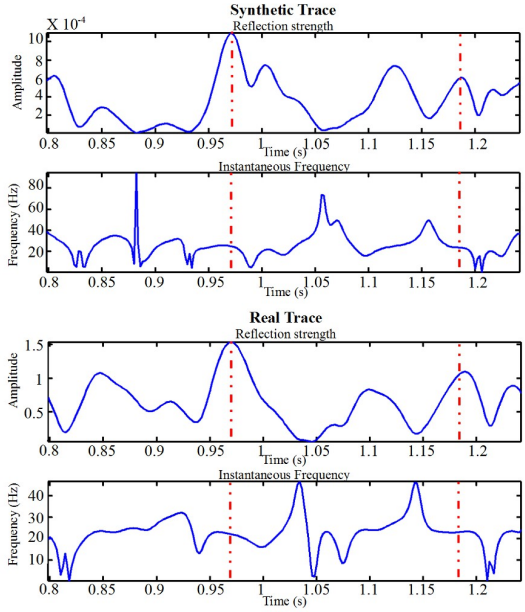

Figure 6: Comparison between complex attribute reflection strength and instantaneous frequency computed on synthetic and real seismic trace for Well 2. The dotted red lines indicate the temporal position of the fractured intervals. Note the anomalous high amplitudes of the reflection strength produced by the fractured zones.

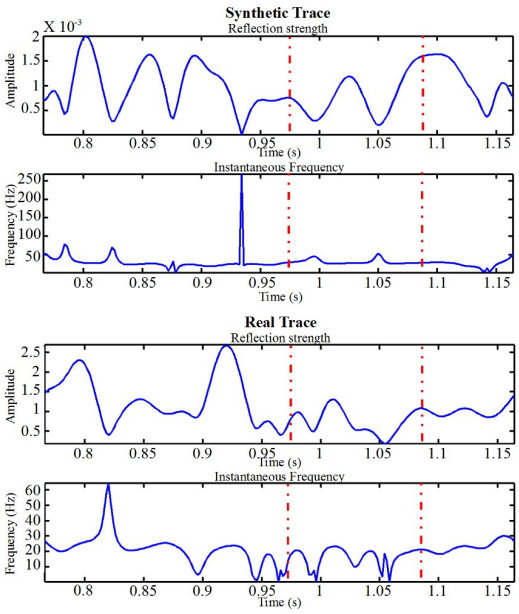

Figure 7: Comparison between complex attribute reflection strength and instantaneous frequency computed on synthetic and real seismic trace for Well 3. The dotted red lines indicate the temporal position of the fractured intervals. Note the anomalous high amplitude of the reflection strength produced by the deeper fractured zone, especially in the synthetic trace.

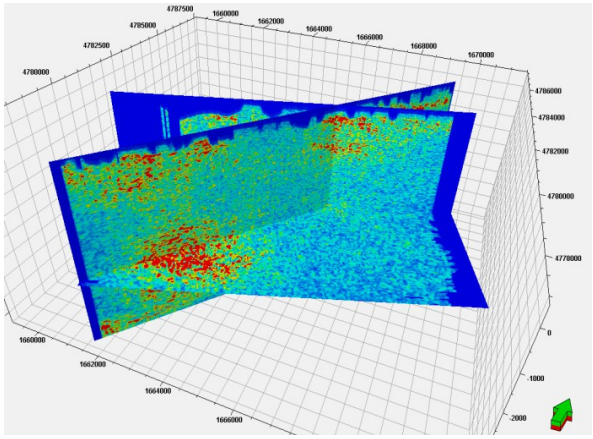

Figure 8: Complex attribute reflection strength computed on the 3D seismic volume. The red color represents the highest values corresponding to the main petrophysical contrasts.

5. A BRIEF REVIEW OF THE AVA AND AVAZ ATTRIBUTES

Concerning AVA theory, Shuey (1985) shows that for relatively small angles of incidence, usually less than 30°, the compressional-wave reflection coefficient *Rpp* can be approximated by an equation of the form:

$$Rpp(\theta)=A+Bsin^2(\theta) \qquad [5]$$

In equation 5, Θ is the angle of incidence, A is the intercept and B is the slope (gradient) of the reflection coefficient. For small perturbations in velocity and density at a reflecting interface, the intercept and gradient can be approximated by:

$$A=\frac{1}{2}\left(\frac{\Delta Vp}{\bar{V}p}+\frac{\Delta\rho}{\bar{\rho}}\right) \qquad [6]$$

and

$$B=\frac{1}{2}\frac{\Delta Vp}{\bar{V}p}-2\left(\frac{\bar{V}s}{\bar{V}p}\right)^2\left(2\frac{\Delta Vs}{\bar{V}s}+\frac{\Delta\rho}{\bar{\rho}}\right) \qquad [7]$$

where, at a given interface, the "bar" terms indicate average quantities and Δ denotes the differences between lower and upper medium parameters. Castagna and Swann (1997) separated the possible AVA responses in four classes based on the value and sign of intercept and gradient. In general, the primary attributes extracted for AVA analysis are the intercept and the gradient, which are obtained from NMO corrected CDP records. These attributes can be used independently, or combined to generate additional AVA attributes (Smith and Gidlow, 1987; Castagna and Smith, 1994). The two latter authors discussed the difference of P and S-waves reflection coefficients (*Rp-Rs*) which would highlight the decrease of P waves reflection coefficient (*Rp*) and the slight increase of the S-wave reflection coefficient (*Rs*) which usually occur at a shale/gas-sand interface. The latter attribute can be easily obtained combining intercept and gradient in the following formula (Wiggins et al., 1983):

$$Rp-Rs=\frac{(A+B)}{2} \qquad [8]$$

The AVAZ methodology is based on the Ruger (Ruger, 1997) approximation of the P-wave reflection coefficients for HTI media valids in case of small contrast in elastic parameters at the reflecting interface, small incidence angle (<30°), and weak anisotropy (δ, ε and γ <<1):

$$R_{pp}^{HTI}(\theta,\phi)\approx R_{pp}^{ISO}(\theta)+\left(\left(\frac{\Delta\delta}{2}+\left(\frac{2\bar{V}s}{\bar{V}p}\right)^2\Delta\gamma\right)\cos^2(\phi)\right)\sin^2(\theta)+\left(\left(\frac{\Delta\epsilon}{2}\right)\cos^4(\phi)+\left(\frac{\Delta\delta}{2}\right)\cos^2(\phi)\sin^2(\phi)\right)\sin^2(\theta)\tan^2(\theta) \qquad [9]$$

Where R_{pp}^{HTI} and R_{pp}^{ISO} are the P-wave reflection coefficient for the HTI and isotropy case, respectively, φ is the azimuth and δ, ε, γ are the Thomsen's anisotropy parameters. Then, from a theoretical point of view, the fracture orientation can be estimated observing the azimuthal variations of the reflection coefficients.

6. EXPECTED AVA AND AVAZ RESPONSES FROM THE FRACTURED LEVELS

6.1 "Analytical" and "Experimental" AVA responses

The log data (*Vp*, *Vs* and density) constitute the input to build blocked models, downscaled to the seismic wavelength, that are then used to compute the AVA intercept and gradient. The well log information we have available allows us to build 1D elastic and isotropic models only. The downscaling is performed making use of the Backus theory (Backus, 1962; Schoenberg and Muir, 1989; Folstad and Schoenberg, 1992), assuming a peak frequency of the seismic signal of 20 Hz and considering a minimum P-wave velocity of 4000 m/s. The resulting equivalent layers have thickness of 20 m.

We first compute intercept and gradient using the Shuey equation for each interface of the blocked models ("analytical" AVA response). Afterwards we compare this AVA response with that obtained from a synthetic CDP computed on the blocked models making use of a reflectivity algorithm ("experimental" AVA response). We perform this test because, as mentioned above, the linearisation that brings to the Shuey equation assumes small incidence angles (less than 30 degree), but also small perturbations in velocity and density at the reflecting interface. In this case we are dealing with a complex system of interconnected fractures of limited space extension and with physical properties often sharply contrasting with the surrounding rocks, as shown in Figures 1, 2 and 3. Moreover, the "analytical" approach does not take into account the effects of wave propagation such as multiple reflections, interference and converted-waves. Therefore, it is advisable to check if the outcomes of the simple "analytical" approach match with the "experimental" results obtained from a more stringent and realistic test.

The intercept-gradient cross-plots of the "analytical" and the "experimental" AVA (Figure 9) show distributions of points that nicely overlaps. In particular, note the fair matching between the "analytical" and the "experimental" responses from the top of the five fractured levels (triangles and little squares, respectively). The observed differences can be mainly ascribed to the limited resolution of the synthetic wavelet, that causes interference effects, and to the presence of multiple and converted waves on the reflectivity seismograms. However, both the "analytical" and the "experimental" responses show that the five fractured levels give rise to a Class IV AVA having negative intercept and positive gradient. Therefore, in terms of seismic signal, they will show a negative polarity at zero offset and amplitudes, in absolute value, decreasing with increasing angle of incidence.

Note that the intercept and gradient responses of these geothermal reservoirs are different from the ones that often occur for many, gas-saturated, silicoclastic

rocks, where the reflections exhibit negative polarities at short offsets but amplitudes that increase in absolute value with increasing angle of incidence, that is a typical Class III AVA. In the examined case the Class IV reflections are generated by the decrease of compressional and shear velocity, as well as of density, which occurs where a localized fractured zone is encased in a tight igneous rock.

In Figure 9, following the relationships presented in Castagna et al. (1998), we also indicate with a dotted red line the background trend, drawn assuming a constant density and a constant *Vp/Vs* equal to 1.8. As is known for classical silicoclastic rocks (Castagna, 1993; Ross, 2000), the farther a reflection lies from the background trend the more likely it can belong to a gas-sand level. This characteristic permits to pinpoint possible gas-sand reflections just observing the intercept-gradient cross-plot. Conversely, in our case the intercept and gradient pertaining to the fractured levels lie very close to the background trend and it would not be possible to identify them as likely due to fractures. This difference with gas-sand exploration, makes it clear we need to seek for a more effective attribute to point out the reflections from the deep fractured geothermal reservoirs.

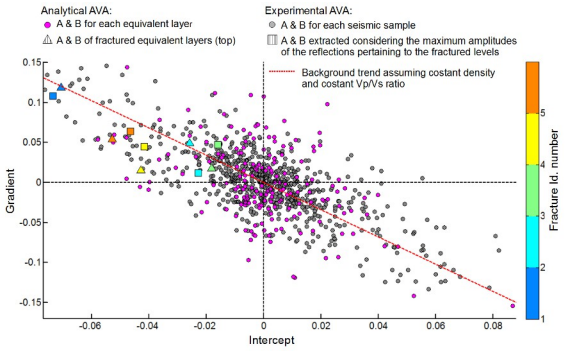

Figure 9: Intercept-Gradient cross-plot of the reflection coefficients computed analytically for all the interfaces of the blocked models (small magenta circles) and of the (scaled) amplitudes vs. angle of the synthetic reflections (small grey circles). The small triangles map the "analytical" response while the small squares refer to the "experimental" response of the top of the fractured levels. The color bar codes the fracture number. Note the fair overlapping of the "analytical" and of the "experimental" responses and the proximity of points (triangles and squares) pertaining to the ("analytical" and "experimental") responses of the fractured levels. Considering the reflections pertaining to the fractured zones we show the Intercept and Gradient extracted considering the peak amplitudes of the wavelets. The dotted red line shows the theoretical "fluid line" assuming constant density and a constant *Vp/Vs* of 1.8.

6.2 An AVA attribute for fracture detention

The decrease of density, *Vp* and *Vs* which occurs passing from the tight rock to the fractured levels also causes the decrease of P and S reflection coefficients *(Rp* and *Rs)*. For this reason, the *Rp-Rs* indicator of equation (8), would not show any anomalous behaviour in our case. However, a very simple modification of this attribute, that is summing the two coefficients *(Rp+Rs)* instead of differentiating them, brings to a more effective detection of fractured levels because their reflections will show anomalously negative values (Aleardi and Mazzotti, 2012). This new AVA attribute can be simply computed using the following formula:

$$Rp+Rs=\frac{(3A-B)}{2} \qquad [10]$$

In Figures 10 and 11 we show the values of *Rp+Rs* computed for each interface of the blocked model ("analytical" AVA) and for each seismic sample ("experimental" AVA), respectively. These figures show that most samples range between values from 0.05 to -0.05, which we may say define the "background" trend, against which all the analysed fracture reflections stand out, having strong negative values of *Rp+Rs* (small triangles in Figure 10, and small squares in Figure 11).

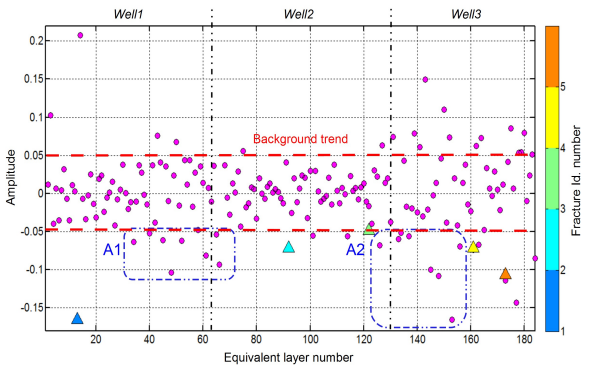

Figure 10: Plot of the *Rp+Rs* coefficients computed analytically for all the interfaces of the blocked models (small magenta circles). The small triangles indicate the "analytical" *Rp+Rs* of the top of the fractured levels. The color bar codes the fracture number. Note that *Rp+Rs* points pertaining to fractures tend to separate from the background (defined approximately by the two dashed horizontal red lines). The *Rp+Rs* coefficients included in the blue rectangles A1 and A2 may pertain to other fractured zones along the well profiles.

Moreover, there are clearly visible two other zones, labelled A1 and A2 in Figure 10 and E1and E2 in Figure 11 (enclosed by the dotted blue rectangles), that represent corresponding depth and time intervals for the "analytical" and the "experimental" responses, respectively. These samples show values of the *Rp+Rs* indicator as low as those pertaining to the

already discovered fractured intervals and might indicate the presence of other fractured levels.

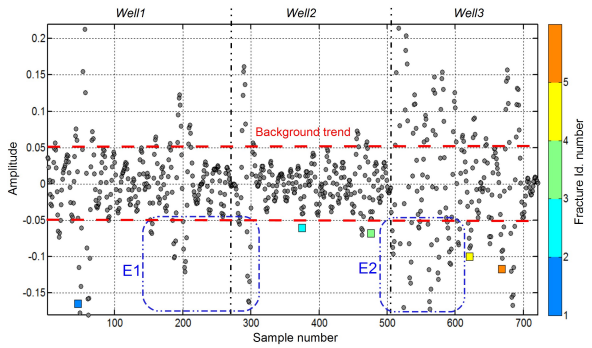

Figure 11: Plot of the *Rp+Rs* coefficients derived from the sample by sample AVA intercept and gradient of the synthetic reflections computed on the blocked models (small grey circles). The little squares indicate the "experimental" *Rp+Rs* pertinent to the fractured levels. The color bar codes the fracture number. As noted for the "analytical" response in the previous figure, the *Rp+Rs* points pertaining to fractures tend to separate from the background. In this case too, two areas indicated by the blue rectangles E1 and E2, that correspond to the same levels within the rectangles A1 and A2 of the previous figure, contain *Rp+Rs* coefficients that may pertain to other fractured zones along the well profiles.

6.3 Expected analytic AVAZ response from the fractured levels

As stated in 6.1 the available information allows us to compute only the isotropy AVA response of the fractured zones. But making some assumptions and considering the recorded P-wave, S-wave velocities and density logs we can also compute the expected AVAZ response of the fractured intervals. The most important assumptions are that the vapour reservoirs in the Larerello-Travale geothermal field, are hosted in vertically aligned fractures (HTI media), totally vapour saturated and embedded in an isotropic background medium. Information concerning the crack density (fracture density per volume) are not available but, if we assume different values for this parameter, some “what if” scenarios can be illustrated. To investigate the variations in seismic P-wave reflection coefficients with offset and azimuth, we compute the compliance tensor and the properties of the equivalent effective HTI medium following Schoenberg and Sayers (1995) and Krasovec et al. (1998). The previously computed elastic constants characterizing the effective medium are then used to compute the Thomsen's parameters (δ, ε and γ), while the Ruger's formula (Equation 9) is applied to model the AVAZ response of the interface separating the overlying isotropic and the underlying HTI media, which contains the fracture set.

We only show the computed AVAZ response for the fracture N.2 found in the Well 2 (Figure 2). For simplicity Figure 12 represents the AVAZ response only for waves propagating parallel to (azimuth=90°) and perpendicular to (azimuth=0°) the fracture set. In the first case the AVAZ response for the HTI medium is equivalent to the isotropy case (Figure 12a) and we see that increasing the crack density from 0 (non fractured, isotropic medium) to 0.1, the intercept shifts towards negative values while the gradient becomes more positive. These effects are due to the increase in physical contrasts at the reflecting interface (strong decrease in seismic velocity and density) produced by the increase in crack density. In Figure 12b the AVAZ responses computed considering an azimuth of 0° are shown. Comparing any reflection coefficient curve with the corresponding curve of Figure 12a, we note that the intercept values are obviously the same, while the gradient assumes stronger positive values for the zero azimuth case. Then, from a theoretical point of view, the spatial orientation of the fracture set can be retrieved comparing the AVA responses for different azimuths.

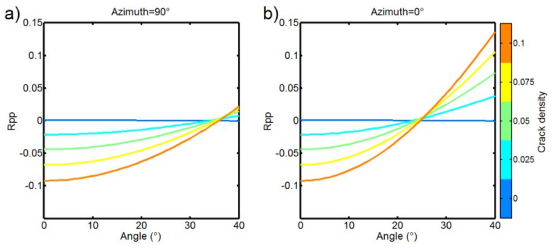

Figure 12: Expected AVAZ response for the fracture N.2 (Well 2) computed considering azimuths equal to 90° and 0° (part a and b, respectively) and different crack densities. Observe the strong variation of the slope of the reflection coefficients with varying azimuth from 90° to 0°.

7. CONCLUSIONS

The deepest geothermal reservoirs in the Larderello-Travale area are hosted in localized fractured zones within the metamorphic basement and intrusive rocks. The reservoir levels are characterized by densities and seismic velocities that sharply decrease with respect to the densities and velocities of the encasing tight rocks. In the analysed case, the reflection strength proves to be the most robust and significant post-stack attribute either in the synthetic data case and in the actual 3D data. Moreover, the studies carried out on the synthetic pre-stack data demonstrate the potential of AVA (Amplitude Versus Angle) analysis and in particular of the P-wave and S-wave reflection coefficient attributes, to detect fractured zones. In fact, the sum of the two attributes *Rp* and *Rs* reaches anomalous values in correspondence of the reflections from the fractured levels. Finally, if we consider a HTI (horizontal transverse isotropic) media, the change of the reflected amplitudes with the source to receiver azimuths shows subtle variations that are due to the presence of quasi-

vertical and aligned fractures. However, a major requirement for the reliable applications of these pre-stack methods to the detection of fractured zones, is the high quality of the pre-stack seismic data. In this sense, the Larderello-Travale seismic data are particularly difficult and thus the post-stack seismic attributes remain the most robust and reliable indicators.

REFERENCES

Adriansyah and McMechan, G.A.: AVA analysis and interpretation of a carbonate reservoir: northwest Java basin, Indonesia, *Geophysics*, **66(3)**, (2001), 744–754.

Aki, K. and Richards, P.G.: Quantitative seismology: Theory and methods, *W. H. Freeman*, (1980).

Aleardi, M. and Mazzotti, A.: A study on the seismic AVO signatures of deep fractured geothermal reservoirs in an intrusive basement, *European Geoscientists Union General Assembly 2012*, Vienna, Austria, (2012), **14**, 3043.

Backus, G.E.: Long-wave elastic anisotropy produced by horizontal layering, *Journal of Geophysical Research*, **67**, (1962), 4427-4440.

Baldi, P., Bertini, G., Cameli, G.M., Decandia, F. A., Dini, I., Lazzarotto, A. and Liotta, D.: La tettonica distensiva post-collisionale nell'area geotermica di Larderello (Toscana meridionale): *Studi Geologici Camerti*, **1**, (1994b), 183-193.

Barbier, E.: Geothermal energy and current status: an overview, renewable and suistainable energy, *Reviews*, **6**, (2002), 3-65.

Batini, F., Cameli, G. M., Lazzarotto, A. and Liotta, D.: Line CROP 18: Southern Tuscany, *Memorie Descrizone Carta Geologica d'Italia*. **62**, (2003), 137-144.

Bertini, G., Cameli, G.M., Costantini, A., Decandia, F. A., Di Filippo, M., Dini, I., Elter, F. M., Lazzarotto, A., Liotta, D., Pandeli, E., Sandrelli, F. and Toro, B.: Struttura geologica fra i monti di Campiglia e Rapolano Terme (Toscana meridionale): stato attuale delle conoscenze e problematiche, *Studi Geologici Camerti*, **1**, (1991), 155-178.

Bertini, G., Casini, M., Gianelli, G. and Pandeli, E.: Geological structure of a long-living geothermal system, Larderello, Italy, *Terra Nova*, **00**, (2006) , 1-7.

Boccaletti, M. and Guazzone, G.: Gli archi appenninici, il mare Ligure ed il Tirreno nel quadro della Tettonica dei Bacini marginali di retro-arco, *Memorie Società Geologica Italiana*, **11**, (1972), 201-216.

Boccaletti, M., Coli, M., Decandia, F.A., Giannini, E. and Lazzarotto, A.: Evoluzione dell' Appennino settentrionale secondo un nuovo modello strutturale, *Memorie Società Geologica Italiana*, **21,** (1981), 359-373.

Carmignani, L. and Kligfield, R.: Crustal extension in the northern Apennines: the transition from compression to extension in the Alpi Apuane core complex, *Tectonics*, **9**, (1990), 1275-1303.

Carmignani, L., Decandia, F.A., Fantozzi, P.L., Lazzarotto, A., Liotta, D. and Meccheri, M.: Tertiary extensional tectonics in Tuscany (Northern Apennines, Italy), *Tectonophysics*, **238**, (1994), 295-315.

Carmignani, L., Decandia, F.A., Disperati, L., Fantozzi, P.L., Lazzarotto, A., Liotta, D. and Oggiano, G.: Relationships between the Sardinia-Corsica-Provençal Domain and the northern Apennines, *Terra Nova*, **7**, (1995), 128-137.

Casini, M., Ciuffi, S., Fiordelisi, A., Mazzotti, A., Perticone, I., Spinelli, E. and Stucchi, E. 3D Seismic for the deep exploration of the travale geothermal field (Italy), I-GET project results, In: *Transactions-Geothermal Resources Council,* Davis, California, **33**, (2009), 915-919.

Casini, M., Ciuffi, S., Fiordelisi, A., Mazzotti, A. and Stucchi, E.: Results of a 3D seismic survey at the Travale (Italy) test site, *Geothermics*, **39**, (2010), 4-12.

Castagna, J.P.: Petrophysical imaging using AVA, *The Leading Edge*, **12-3**, (1993), 172-179.

Castagna J.P. and Smith S.W.: Comparison of AVO indicators: A modeling study. *Geophysics*, **59**, (1994), 1849-1855.

Castagna, J.P. and Swan H.W.: Principles of AVO crossplotting, *The Leading Edge*, **16**, (1997), 337–342.

Castagna J.P., Swan, H.W. and Foster, D. J.: Framework for AVO gradient and intercept interpretation, *Geophysics*, **63**, (1998), 948–956.

Fatti, J.L., Smith, G.C., Vail, P.J., Strauss, P.J. and Levitt, P.R.: Detection of Gas in Sandstone Reservoirs Using AVA Analysis: a 3-D Seismic Case History Using the Geostack Technique, *Geophysics*, **59**, (1994), 1362-1376.

Folstad P.G. and Schoenberg M.: Use of equivalent anisotropic medium theory to calculate synthetic AVO response: Abstract on "How useful is AVO analysis?", *Joint SEG/EAGE Summer Research Workshop*, (1992), 614-621.

Gray, D., Head, K.J., Chamberlain, C.K., Olson, G., Sinclair, J. and Besler, C.: Strike Analysis: A Core Matter, *AAPG Explorer*, **9**, (1999).

Jolivet, L., Dubois, R., Fournier, R., Goffe', B., Michard, A. and Jourdan, C.: Ductile extension in alpine Corsica, *Geology*, **18**, (1990), 1007-1010.

Jolivet, L., Faccenna, C., Goffe', B., Mattei, M., Brunet, C., Rossetti, F., Cadet, J.P., Funiciello, R.,

Theye, T., Storti, F. and D'Agostino, N.: Mid-crustal shear zones in postorogenic extension: Example from the Northern Tyrrhenian Sea., *Journal of Geophysical Research*, **103**, (1998), 12213-12160.

Krasovec, M., Rodi, W. and Toksöz, M.: Sensitivity analysis of amplitude variation with offset (AVO) in fractured media, *SEG Technical Program Expanded Abstracts*, (1998), 201-203.

Lynn, H.B., Simon, K.M. and Bates, C.R.: Correlation between P-wave AVOA and S-wave traveltime anisotropy in a naturally fractured gas reservoir, *The Leading Edge*, **15-8**, (1996), 931-935.

Mallick, S., Craft, K.L., Meister, L.J. and Chambers, R. E.: Determination of the principal directions of azimuthal anisotropy from P-wave seismic data., *Geophysics*, **63**, (1998), 692-706.

Mazzotti A.: Prestack amplitude analysis methodology and application to seismic bright spots in the Po Valley, Italy, *Geophysics*, **55**, (1990), 157-166.

Mazzotti A.: Amplitude, Phase and Frequency versus Offset Applications, G*eophysical Prospecting*, **39**, (1991), 863-886.

Mazzotti A., Zamboni, E., Stucchi, E. and Ciuffi, S.: Seismic characterisation of geothermal reservoirs - a case study in western Tuscany, Italy, *EAGE 64th Conference and Technical Exhibition*, Extended Abstracts, (2002), C037.

Ostrander, W.J.: Plane-wave Reflection Coefficients for Gas Sands at Non-normal Angles of Incidence, *Geophysics*, **49**, (1984), 1637-1648.

Ross, C.P.: Effective AVO crossplot modeling: A tutorial, *Geophysics*, **65**, (2000), 700–711.

Rüger, A.: P-wave reflection coefficients for transversely isotropic models with vertical and horizontal axis of symmetry, *Geophysics*, **62**, (1997), 713–722.

Rutherford, S.R. and Williams, R.H.: Amplitude versus-offset variations in gas sands, *Geophysics*, **54**, (1989), 680-688.

Schoenberg, M. and Muir, F.: A calculus for finely layered anisotropic media, *Geophysics*, **54**, (1989), 581-589.

Schoenberg, M. and Sayers, C.M.: Seismic anisotropy of fractured rock, *Geophysics,* **60**, (1995), 204–211.

Shen F., Sierra*z* J., Burns D.R., and Toksöz, M.N.: Azimuthal offset-dependent attributes applied to fracture detection in a carbonate reservoir, *Geophysics*, **67**, (2002), 355–364.

Shuey, R.T.: A simplification of the Zoeppritz equations, *Geophysics*, **50**, (1985), 609–614.

Smith, G.C. and Gidlow, P.M.: Weighted stacking for rock property estimation and gas detection, *Geophysical Prospecting*, **35**, (1987) 993–1014.

Taner M.T., Koeler, F. and Sheriff, R.E.: Complex seismic trace analysis, *Geophysics*, **44**, (1979), 1041-1063.

Thomsen, L.: Weak elastic anisotropy, *Geophysics*, **51**, (1986), 1954-1966.

Wiggins, R., Kenny, G.S. and McClure, C.D.: A method for determining and displaying the shear-velocity reflectivities of a geologic formation: *European Patent Application*, (1983), 0113944.